

1 **BrGDGTs-based seasonal paleotemperature reconstruction for the last 15,000 years**
2 **from a shallow lake on the eastern Tibetan Plateau**

3 Xiaohuan Hou ^a, Nannan Wang ^a, Zhe Sun ^b, Kan Yuan ^{a,c}, Xianyong Cao ^a, Juzhi Hou ^{a*}

4 ^a *Group of Alpine Paleocology and Human Adaptation (ALPHA), State Key Laboratory of Tibetan*
5 *Plateau Earth System, Resources and Environment (TPESRE), Institute of Tibetan Plateau Research,*
6 *Chinese Academy of Sciences, Beijing 100101, China*

7 ^b *Institute of Geography and Resources Science, Sichuan Normal University, Chengdu, 610066, China*

8 ^c *University of Chinese Academy of Sciences, Beijing 100049, China*

9

10 * Corresponding author

11 E-mail address: houjz@itpcas.ac.cn

12

13 **ABSTRACT**

14 Knowledge of Holocene temperature changes is crucial for addressing the problem of the
15 discrepancy between Holocene proxy temperature reconstructions and climate model
16 simulations. The complex spatiotemporal pattern of temperature variations on the Tibetan
17 Plateau (TP) further complicates the study of Holocene continental climate change. The
18 discrepancy between model-based and proxy-based Holocene temperature reconstructions
19 possibly results from the seasonal biases and environmental ambiguities of the proxies.
20 Quantitative temperature reconstructions using different proxies from the same sediment core
21 can provide an effective means of evaluating different proxies; however, this approach is
22 unusual in terrestrial environments. Here, we present an ice-free-season temperature record
23 for the past 15 ka from a shallow, freshwater lake on the eastern TP, based on brGDGTs
24 (branched glycerol dialkyl glycerol tetraethers). This record shows that the Holocene Thermal
25 Maximum lags the pollen-based July temperature recorded in the same sediment core. We
26 conclude that the mismatch between the brGDGTs-based and pollen-based temperatures is
27 primarily the result of seasonal variations in solar irradiance. The overall pattern of
28 temperature changes is supported by other summer temperature records, and the Younger
29 Dryas cold event and the Bølling–Allerød warm period are also detected. A generally warm
30 period occurred during 8–3.5 ka, followed cooling in the late Holocene. Our findings have
31 implications for understanding the seasonal signal of brGDGTs in shallow lakes, and provide
32 critical data for confirming the occurrence of seasonal biases in different proxies from high-
33 elevation lakes. To further investigate the significance of the brGDGTs and temperature
34 patterns on the TP, we reviewed previously published brGDGTs-based Holocene temperature

35 records across the TP. The results demonstrate that brGDGTs have been employed to
36 reconstruct various temperatures in different studies, including annual average temperature
37 and warm-biased temperature.~~The results demonstrate that brGDGTs can record both annual~~
38 ~~mean temperature and a warm-biased temperature,~~ and that both show a gradual warming
39 trend during the Holocene with relatively cooler conditions during the middle Holocene, and
40 a cooling trend during the middle to late Holocene. We analyzed the possible reasons for the
41 diverse brGDGTs records on the TP and emphasize the importance of considering lake
42 conditions and modern investigations of brGDGTs in lacustrine systems when using
43 brGDGTs to reconstruct paleoenvironmental conditions.

44 **Keywords:** Tibetan Plateau, brGDGTs, the mean temperature of Months Above
45 Freezing warm-biased temperature, shallow lake, Holocene

46 **1 Introduction**

47 Global climate change has had a profound impact on both the natural ecological and socio-
48 economic systems that are vital for human survival and development, making climate change
49 a critical limiting factor for the sustainable development of human society. The Tibetan
50 Plateau (TP), also called the “Third Pole” (Qiu, 2008), has undergone, a more rapid warming
51 over the last five decades, with a rate twice that of the global average (0.3 – 0.4°C/decade)
52 (Chen et al., 2015; Kuang and Jiao, 2016), making it one of the world's most temperature-
53 sensitive regions (Chen et al., 2015; Yao et al., 2022). Consequently, assessing the impact of
54 future climate change on the TP is becoming increasingly important. To enhance the
55 precision and accuracy of future climate change estimates for the TP under ongoing global
56 climate change and to minimize the uncertainty in climate simulations, it is essential to

设置了格式: 字体颜色: 深红

57 investigate the processes and mechanisms of regional climate and environmental changes,
58 with particular emphasis on temperature, on a relatively long timescale, such as that of the
59 Holocene.

60
61 The Holocene, the most recent geological epoch, is closely linked with the development of
62 human civilization. Quantitative reconstructions of Holocene temperature trends can be used
63 to explore their impacts on civilization and to establish a geological and historical context for
64 predicting future climate changes. In recent decades, ~~several~~ many Holocene quantitative

设置了格式: 字体颜色: 深红

65 reconstructions of seasonal and annual temperatures for the TP have been produced using
66 various proxies, like pollen (Herzschuh et al., 2014; Lu et al., 2011), chironomids (Zhang et
67 al., 2017; Zhang et al., 2019a), $\delta^{18}\text{O}$ in ice ~~deposits~~ cores (Pang et al., 2020; Thompson et al.,

设置了格式: 字体颜色: 深红

68 1997), and biomarkers (Cheung et al., 2017; Hou et al., 2016; Zhao et al., 2013). These
69 reconstructions have provided crucial data for the elucidation of Holocene temperature
70 changes. However, the available Holocene temperature records from the TP show divergent
71 trends. Multiple proxy indicators indicate three different Holocene temperature patterns on
72 the TP. First, a consistent Holocene warming trend (Feng et al., 2022; Opitz et al., 2015; Sun
73 et al., 2022). For example, brGDGTs based annual temperatures (Feng et al., 2022; Sun et al.,
74 2022) indicate a gradual warming trend which resembles the $\delta^{18}\text{O}$ temperature record from
75 the Chongce ice core on the western TP, except for the last 2 ka (Pang et al., 2020). Second,
76 an early to middle Holocene summer temperature maximum and a gradual cooling trend
77 during the late Holocene are observed in pollen-, alkenone- and chironomid-based
78 temperature records (Herzschuh et al., 2014; Hou et al., 2016; Wang et al., 2021a; Zhang et
79 al., 2017; Zheng et al., 2015). Third, a prominent relatively cool middle Holocene (Li et al.,

80 2017; Wang et al., 2021c); for example, a composite temperature record suggests that
81 temperatures were ~2°C cooler during the middle Holocene than during the early and late
82 Holocene (Wang et al., 2021c). Several records also show a steady long-term trend without
83 distinct cooling or warming (Sun et al., 2021). Moreover, the cooling trends in proxy-based
84 Holocene temperature records are inconsistent with those of climate models, which indicate a
85 warming trend, and this inconsistency is widely known as the “Holocene temperature
86 conundrum” (Liu et al., 2014). There are several potential factors that may contribute to the
87 disparity in Holocene temperature trends, including seasonal biases and uncertainties in
88 temperature proxies and reconstructions, independent of climate models (Bova et al., 2021;
89 Cartapanis et al., 2022; Hou et al., 2019; Liu et al., 2014; Marsicek et al., 2018). While
90 several recent studies have suggested that seasonality in proxies is not the major cause of the
91 Holocene temperature conundrum (Dong et al., 2022; Zhang et al., 2022b), it is significant
92 that the TP is an alpine and high-altitude region with significant seasonal temperature
93 variations. Moreover, most organisms tend to grow during the warmer seasons at high
94 latitudes and high altitudes (Zhao et al., 2021a). Currently, however, we lack unambiguous
95 and reliable seasonal temperature records to support a seasonality-bias hypothesis. Extensive
96 research has been conducted in lakes, employing a single proxy to reconstruct past
97 temperature fluctuations. However, there have been scarce studies that employ various
98 proxies within the same core to reconstruct paleotemperature variations. Furthermore, the
99 limited number of studies primarily concentrate on reconstructing summer temperature and
100 annual average temperature. Most previous studies have relied on a single temperature proxy,
101 and the few studies that have used multiple proxies from the same sediment core have tended

设置了格式：字体颜色：深红

102 ~~to focus on annual average temperature and summer temperature.~~ For example, a chironomid-
103 based July temperature reconstruction for Tiancai lake on the southeastern TP shows higher
104 temperatures during the early to middle Holocene (Zhang et al., 2017), while the brGDGTs-
105 based annual average temperature shows a warming trend (Feng et al., 2022). Different
106 proxies may reflect the seasonal temperatures in different months, and thus producing
107 temperature reconstructions for different months for the same sediment core may help better
108 understand the seasonal bias of terrestrial temperature records. Furthermore, the
109 reconciliation of the divergent trends of Holocene temperature on the TP and its surroundings
110 requires additional high-altitude temperature records from these regions, with reliable
111 chronologies and proxy records with an unambiguous climatological significance.

112
113 Branched glycerol dialkyl glycerol tetraethers (brGDGTs) are a group of membrane-spanning
114 lipids found in bacteria (Fig. S1) (Chen et al., 2022; Halamka et al., 2022; Sinnighe Damsté
115 et al., 2000), and they have become a powerful tool for quantifying past terrestrial
116 temperature variations. Through investigations of brGDGTs in globally-distributed soils, it
117 was found that the distribution of brGDGTs is primarily related to temperature and pH
118 (Weijers et al., 2007). Subsequently, brGDGTs–temperature calibrations from soil, peat and
119 lake sediments were established on scales from global (Crampton-Flood et al., 2020; De
120 Jonge et al., 2014; Martínez-Sosa et al., 2021; Weijers et al., 2007) to regional (e.g., East Asia)
121 (Dang et al., 2018; Ding et al., 2015; Sun et al., 2011; Wang et al., 2016), leading to
122 ~~considerable~~ significant progress in reconstructing terrestrial temperatures, particularly on the
123 TP (Cheung et al., 2017; Li et al., 2017; Zhang et al., 2022a).

124

125 Natural lakes are widely distributed across the TP (Zhang et al., 2019b). Lake sediments,
126 characterized by their organic matter-rich composition, exhibit continuous and rapid
127 accumulation rates. As a result, they offer high-resolution records of environmental changes,
128 making them highly valued as a primary terrestrial climate archive.~~Lake sediments are often~~
129 ~~organic matter rich and they accumulate continuously and rapidly, providing high resolution~~
130 ~~records of environmental change, and they are thus regarded as the most important terrestrial~~
131 ~~climate archive~~ (Moser et al., 2019). BrGDGTs in lacustrine systems are often more strongly
132 correlated with temperature, with higher coefficient of determination (r^2) and lower root
133 mean square error (RMSE) values (Martínez-Sosa et al., 2021), than in soils and peats.
134 However, the factors that impact the distribution of brGDGTs in lakes are intricate and
135 multidimensional. Notably, the sources of brGDGTs within lakes are intricate, involving
136 contributions from soil as well as autochthonous lake processes. Moreover, an expanding
137 body of research underscores a substantial prevalence of autochthonous brGDGTs in lakes
138 (Tierney and Russell, 2009; Tierney et al., 2010; Wang et al., 2021b; Weber et al., 2015).
139 Furthermore, the origins of brGDGT producers remain uncertain and could be influenced by
140 various factors, including lake salinity (Wang et al., 2021b), redox conditions (Weber et al.,
141 2018), oxygen content and/or mixing patterns (Wang et al., 2021b) (Weber et al., 2018)
142 (Buckles et al., 2014; van Bree et al., 2020; Wu et al., 2021). Additionally, even lake depth
143 plays a role due to distinct ecological niches (Woltering et al., 2012), thereby contributing to
144 the intricate interplay that shapes the distribution of brGDGTs within lakes.~~(Woltering et al.,~~
145 ~~2012)~~ However, the factors influencing the distribution of brGDGTs in lakes are complex and

设置了格式：字体颜色：深红

146 multidimensional; moreover, as well as temperature and pH, other factors like salinity (Wang
147 et al., 2021b), oxygen content (Buckles et al., 2014), and water depth (Woltering et al., 2012)
148 can significantly impact the distribution of brGDGTs in lakes.

149
150
151

152 In this study, we obtained a quantitative temperature reconstruction for the past 15 ka from
153 Gahai, a shallow (average depth of ~2 m) freshwater lake located in the source area of the
154 Yellow River. This region is an important ecological protection area on the eastern edge of
155 the TP. Freshwater environments avoid the confounding effects of salinity on brGDGTs-
156 based temperature reconstructions, and shallow lakes also minimize the impact of the uneven
157 distribution of light and nutrients on brGDGTs. Our specific aims were: (1) to determine the
158 long-term trend of Holocene warm-biased terrestrial temperatures at a high elevation; (2) to
159 compare records of ice-free season temperatures with July temperatures from the same
160 sediment core; and (3) to gain a better understanding of the possible mechanisms responsible
161 for Holocene temperature variations, especially on the TP.

162 **2 Materials and methods**

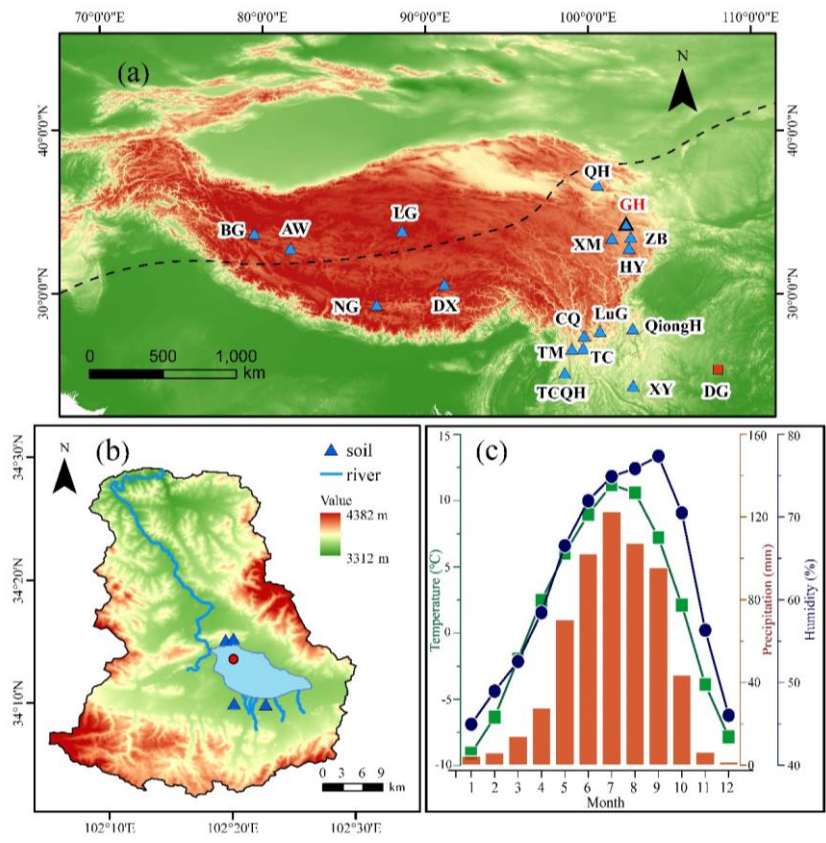
163 *2.1 Study site*

164 Gahai (102°11'–102°28' E, 34°04'–34°4' N, 3444 m a.s.l.) is a freshwater lake and part of the
165 Gahai meadow wetland, which is a national nature reserve with restricted human access, on
166 the eastern edge of the Tibetan Plateau (Fig. 1). The lake is fed by runoff from the
167 surrounding hills, and it drains into the Tao river, which ultimately enters the

168 Yellow ~~river~~River. Thus, Gahai lake is a critical water conservation area in the upper reaches
169 of the Yellow River. The average water depth of Gahai is ~1–2 m, and the maximum depth is
170 ~5 m. The vegetation in the catchment consists mainly of *Kobresia tibetica*, *Equisetum*
171 *arvense*, *Potentilla anserina*, *Artemisia subulate*, and *Oxytropis falcata* (Ma et al., 2019).
172 Meteorological data for the area are available from Langmu Temple station (1957-1988) (Fig.
173 1) (102°38' E, 34°5' N, 3412 m a.s.l.), ~32 km northwest of Gahai lake. They indicate an
174 annual average (mean) precipitation of 781 mm, with > 67% occurring between June and
175 September, and mean annual temperature of 1.2 °C with a relative humidity of ~65%. The
176 summers are mild and humid and the winters are cold and dry. From May to September, the
177 mean average temperature is above freezing (0°C), but the temperature in May is very low,
178 close to 0°C.

设置了格式: 字体颜色: 深红

设置了格式: 字体颜色: 深红



179
 180 **Fig. 1** (a) Locations of the sites on the Tibetan Plateau referenced in the text. Triangle with
 181 bold line indicates the location of Gahai lake (this study). Other triangles indicate the
 182 locations of cited studies on the Tibetan Plateau and the surrounding area: Bangong Co
 183 (BG), Aweng Co (AW), Ngamring Co (NG), Linggo Co (LG), Dangxiong wetland (DX),
 184 Qinghai lake (QH), Ximen Co (XM), Zoige Basin (ZB), Hongyuan peatland (HY), Lugu
 185 lake (LuG), Cuoqia lake (CQ), Tingming lake (TM), Tengchongqinghai lake (TCQH),
 186 Tiancai lake (TC), Qionghai lake (QH), Xingyun lake (XY). Red square indicates
 187 Dongge Cave (DG). Black dotted line represents the northern boundary of the modern
 188 Asian summer Monsoon (Chen et al., 2008). (b) Drainage basin of Gahai lake and the
 189 core site. (c) Climate data from Langmu Temple meteorological station: monthly
 190 temperature (green line), precipitation (red bars), and humidity (blue line).

191 2.2 Sampling

192 A sediment core with the length of 329 cm was obtained from Gahai Lake in January 2019, at
193 a water depth of 1.95 m, using a UWITEC platform operated from the frozen lake surface. In
194 addition, ~~several~~four catchment soil samples were collected from around the lake (Fig. 1).
195 All samples were transported to the Institute of Tibetan Plateau Research, Chinese Academy
196 of Sciences (ITPCAS). The sediment core was split lengthwise, and one half was subsampled
197 and freeze-dried for subsequent analysis.

设置了格式: 字体颜色: 深红

设置了格式: 字体颜色: 红色

198

199 2.3 Chronology

200 The chronology of the upper 20 cm of the sediment core is based on measurements of ^{210}Pb
201 and ^{137}Cs , at a 1-cm interval. The chronology for the deeper part of the core is provided by
202 accelerator mass spectrometry (AMS) ^{14}C measurements of 13 bulk sediment samples, which
203 were conducted by Beta Analytic Inc. (Miami, USA) (Fig. 2) (Wang et al., 2022).

204

205 The ^{210}Pb age model was constructed using the constant rate of supply (CRS) model and the
206 ^{137}Cs peak was used as supplement (Appleby, 2002). The calculated age of ^{210}Pb using CRS
207 model aligned well with the ^{137}Cs peak at 6 cm. Overall, the CRS model was deemed suitable
208 for determining the age of Gahai lake.

设置了格式: 字体颜色: 深红

209

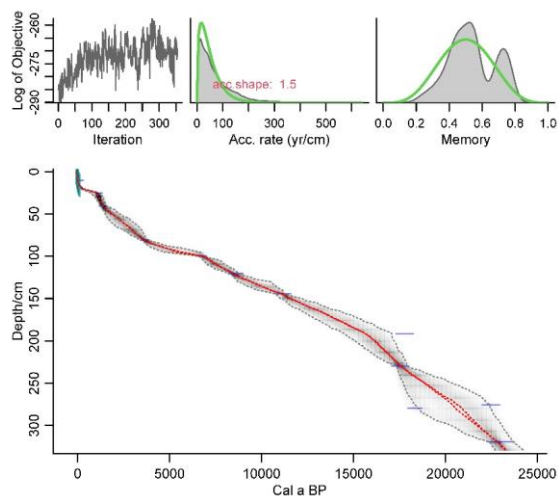
210 Reservoir age, as highlighted by Hou et al. (2012), is a crucial factor affecting the age
211 determination of lake sediment cores on the TP. Therefore, it was necessary to establish the
212 reservoir age of Gahai lake before undertaking paleoclimate reconstruction. The linear

设置了格式: 字体颜色: 深红

带格式的: 行距: 2 倍行距

213 extrapolation relationship between the ^{14}C ages and depth to the sediment-water interface is
214 often used to estimate the reservoir age. The ^{14}C age of 13 samples exhibits a good linear
215 relationship with sediments depth in Gahai lake. Extrapolation of this 13 ^{14}C ages down to the
216 depth of 6 cm yielded a ^{14}C age of 461 yr BP, while the reliable ^{210}Pb age at 6 cm is -27 yr BP.
217 Consequently, the difference between the two ages, which amounts to 488 yr, was taken as
218 the reservoir age. Additionally, it's worth noting that independent estimations of the ^{14}C
219 calibration age and ^{210}Pb age around 10 cm in Gahai lake was obtained, resulting in values of
220 497 yr BP and 18 yr BP, respectively. The difference of 479 yr between these two ages can
221 also be considered as the reservoir age. These two methods of estimating reservoir age of
222 Gahai lake show very close, which are mutually supportive. So, the average of 483 yr was
223 adopted as the reservoir age. All original ^{14}C dates were corrected by subtracting the reservoir
224 age (483 yr) and calibrating them to calendar ages using Calib 8.1. The age-depth model (Fig.
225 2) was constructed using the Bacon program with the ^{14}C ages and ^{210}Pb ages (Blaauw and
226 Andres Christen, 2011) and was reported by Wang et al. (2022).

▲ 设置了格式：字体颜色：深红



228
 229 **Fig. 2** Age-depth model for Gahai, based on AMS ^{14}C , ^{210}Pb and ^{137}Cs ages (Wang et al.,
 230 2022). The ages of the upper 20 cm are based on ^{210}Pb and ^{137}Cs dating (green symbols)
 231 and those of the lower part on AMS ^{14}C dates (blue symbols).

232

233 2.4 Lipids extraction and brGDGTs analysis

234 For lipids extraction, ~5 g samples were ground to a powder and extracted ultrasonically with
 235 dichloromethane (DCM): methanol (MeOH) (9: 1, v: v) three times. The supernatants were
 236 combined and dried under a stream of nitrogen gas. Subsequently, the total lipid extracts were
 237 separated into neutral and acid fractions through a LC-NH₂ silica gel column using DCM:
 238 isopropyl alcohol (2: 1, v: v) and ether with 4% acetic acid (v: v), respectively. The neutral
 239 fraction was then eluted through a silica gel column using n-Hexane, DCM and MeOH, and
 240 the GDGTs were dissolved in the MeOH. The GDGTs fraction was passed through a 0.45 μm
 241 polytetrafluoroethylene (PTFE) filter before analysis. C₄₆-GDGT (a standard compound)
 242 (Huguet et al., 2006) was added to the samples before analysis.

243

244 BrGDGTs were detected using an HPLC-APCI-MS (Waters ACQUITY UPLC I-Class/Xevo
245 TQD) with auto-injection at the ITPCAS. The compounds were separated by three Hypersil
246 Gold Silica LC columns in sequence (each 100 mm × 2.1 mm, 1.9 μm, Thermo Fisher
247 Scientific; USA), maintained at a temperature of 40°C. GDGTs were eluted isocratically
248 using 84% hexane and 16% ethyl acetate (EtOA) for the first 5 min, followed by a linear
249 gradient change to 82% hexane and 18% EtOA from 5 to 65 min. The columns were cleaned
250 using 100% EtOA for 10 min, and then back to 84% hexane and 16% EtOA to equilibrate the
251 column, with a flow rate of 0.2 ml min⁻¹.

252

253 The APCI-MS conditions were as follows: nebulizer pressure at 60 psi, APCI probe
254 temperature at 400°C, drying gas flow rate of 6 L/min and temperature of 200°C, capillary
255 voltage of 3600 V, source corona of 5.5 μA. Detection was performed in selected ion
256 monitoring (SIM) mode, targeting the protonated molecules at m/z 1050, 1048, 1046, 1036,
257 1034, 1032, 1022, 1020, 1018 and 744. The results were analyzed using MassLynx V4.1
258 software, and quantification was achieved by comparing the peak areas of targeted ions and
259 the internal standard, assuming an identical response factor for GDGTs.

260

261 **3 Results and Discussion**

262 *3.1. Concentration and distribution of brGDGTs in the sediment core and catchment soils*

263 BrGDGTs were detected in both the catchment soils and the downcore sediments. The
264 average concentration of brGDGTs in the catchment soils (0.07 ng g⁻¹dw) was ~~significantly~~
265 ~~higher~~ lower than in the surficial core sediments (0.70 ng g⁻¹dw). In the soil samples,

266 pentamethylated brGDGTs were generally the most ~~abundance~~ (55.33%), followed by
267 tetramethylated brGDGTs (23.60%) and hexamethylated brGDGTs (21.07%) (Fig. S2). The
268 relative amount of cyclopentane ring-containing brGDGTs in the soil samples was generally
269 low (24.34%) and it was sometimes too low to be detected, especially the fractions of IIIb,
270 IIIb', IIIc, IIIc', IIc and IIc'. In the downcore sediments, the relative abundance of
271 tetramethylated brGDGTs (43.84%) was like that of pentamethylated brGDGTs (41.93%),
272 and hexamethylated brGDGTs were the least ~~abundance~~ (14.22%) (Fig. S2). The relative
273 abundant of cyclopentane ring-containing brGDGTs in the downcore sediments (67.82%)
274 was lower than that in the catchment soils.

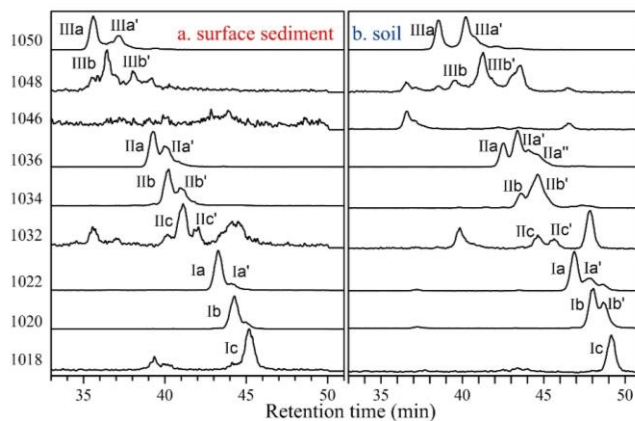
设置了格式: 字体颜色: 深红

275 3.2 *In situ* production of brGDGTs in Gahai lake

276 Although lacustrine brGDGTs have great potential for quantitatively reconstructing terrestrial
277 paleotemperatures, uncertainties about their sources in lacustrine environments are a major
278 factor limiting their application (Buckles et al., 2014; Cao et al., 2020; Sinnighe Damsté et
279 al., 2009; Sun et al., 2011; Tierney and Russell, 2009). To investigate the origin and
280 characteristics of brGDGTs in the Gahai lake sediments, we examined the distributions and
281 concentrations of brGDGTs in the sediments and catchment soils and found
282 ~~notable~~ differences between them. First, as described in the previous section, the
283 average content of brGDGTs in the catchment soils was ~10% that of the surficial lake
284 sediments, suggesting the absence of large-scale allochthonous inputs from the catchment
285 soils. Second, the brGDGTs distributions in the downcore sediments were quite different
286 from those in the catchment soils, which suggests a ~~substantial~~ autochthonous
287 brGDGTs contribution to the lake sediments (Fig. 3 and Fig. S2). Moreover, the ratios of 6-

设置了格式: 字体颜色: 深红

288 methyl brGDGTs to 5-methyl GDGTs (IR_{6ME}) in the soils and sediments, calculated
 289 according to the formula proposed by De Jonge et al. (2014), were ~~significantly~~ different. In
 290 the soil samples, IR_{6ME} varied between 0.54 and 0.57 and the average ratio in the downcore
 291 samples was 0.26, varying between 0.18 and 0.47. Third, the in-situ production of brGDGTs
 292 in Gahai lake is suggested by the discrepancies in the degree of methylation (MBT'_{5ME})
 293 between the soils and surface sediments. The average value of MBT'_{5ME} in the Gahai lake
 294 surface sediments was 0.48, which is clearly higher than in the catchment soils, with the
 295 range of 0.32–0.35. Fourth, and potentially the most significant, the IIIb' and Ib' compounds
 296 are present in the catchments soil but not in the Gahai lake surficial sediments, which may be
 297 direct evidence of an autochthonous brGDGTs contribution in the lacustrine environment
 298 (Fig. 3), and a lower proportion of soil-derived brGDGTs input. Therefore, we conclude that
 299 the brGDGTs in the Gahai lake sediments are mainly of in-situ origin.



300
 301 **Fig. 3** Representative high-performance liquid chromatography/atmospheric pressure
 302 chemical ionization-mass spectrometry (HPLC/APCIMS) chromatograms of brGDGTs
 303 from (a) surface sediments from Gahai lake, and (b) soils in the catchment of Gahai lake.

304

305 *3.3 brGDGTs-temperature calibration and Holocene temperature reconstruction*

306 Gahai is a shallow lake in the eastern Tibetan Plateau that is typically completely frozen
307 during winter and spring. Local meteorological data indicate that the average snowfall period
308 lasts for 269 days, with around 50 days of continuous snowfall (Luqu County Local
309 Chronicles Compilation Committee, 2006). The freezing of the lake surface begins in late
310 October each year and gradually thaws starting from May of the following year. As a result,
311 the light transmittance and oxygen content in the lake water are reduced during the freezing
312 season, leading to decreased nutrient levels, which severely hinder the growth of autotrophic
313 microorganisms. Although the bacteria responsible for producing brGDGTs have not been
314 thoroughly characterized, the abundance of heterotrophic bacteria will likely decrease due to
315 the reduced autotrophic biomass during the winter and spring ice-covered period. The
316 weakened light penetration, decreased oxygen levels, and lack of nutrient replenishment
317 during the frozen period significantly impact the growth of autochthonous microorganisms.

318

319 While the specific bacterial species responsible for brGDGT production are not yet well
320 understood, it is known that these bacteria, as heterotrophic organisms, will also be
321 influenced by the reduction in autotrophic biomass. Furthermore, some research suggests that
322 the production of brGDGTs might be related to factors such as water depth, seasonal
323 alternation of water column mixing and stratification (Loomis et al., 2014; van Bree et al.,
324 2020). During the summer and autumn seasons when the lake ice melts and the water
325 becomes more mobile, the nutrient content increases, resulting in elevated lake biomass.

设置了格式: 字体颜色: 红色

326 moreover, the oxygen levels at the bottom of Gahai lake are not expected to be too high,
327 which could further contribute to the proliferation of brGDGT-producing bacteria, potentially
328 leading to an increase in the brGDGT-producing bacteria (Weber et al., 2018). Therefore,
329 brGDGTs in Gahai lake may provide records of the average temperature during the ice-free
330 months of the summer and autumn seasons.

331
332 Additionally, the presence of the frozen lake surface during winter creates a thermal barrier,
333 impeding the exchange of heat between the lake water and the atmosphere. Consequently,
334 any brGDGTs generated within the lake water during this period lose their ability to
335 accurately reflect atmospheric temperature variations (Sun et al., 2021; Zhang et al., 2022a).
336 Thus, they were no longer able to track atmospheric temperature changes during the frozen
337 season. So, we prefer to use Gahai brGDGTs to reconstruct temperatures during the summer
338 and ice-free seasons. For this purpose, we employed the new Bayesian calibration for the
339 mean temperature of the Months Above Freezing, as proposed by Martínez-Sosa et al. (2021),
340 to derive a warm-biased temperature for Gahai lake.

341
342 To assess the accuracy of this calibration approach, we compared the fractional abundances
343 of summed tetra-, penta-, and hexamethylated brGDGTs in Gahai lake sediments with other
344 datasets (Fig. 4). These datasets include lake sediments from the Tibetan Plateau (Günther et
345 al., 2014; Wang et al., 2016), East Africa (Russell et al., 2018), and global lakes (Martínez-
346 Sosa et al., 2021). The distribution pattern of Gahai core sediments is distinctly remarkable
347 compared to that of other lake sediments within the Tibetan Plateau, even though they share a

348 common regional origin (Fig. 4). However, its resemblance to the global distribution of
349 brGDGTs in lake sediments is evident. Notably, the calibration developed by Martínez-Sosa
350 et al. (2021) is based on brGDGTs from a global lake dataset.

设置了格式: 字体颜色: 深红

351
352 Using calibration of Martínez-Sosa's et al. (2021), we reconstructed the surface sediment
353 temperature of Gahai lake, resulting in a temperature estimate of 9.4°C. This reconstructed
354 temperature closely matches the ice-free season temperature recorded by meteorological
355 stations in the Gahai region (8.8°C for May to September). Furthermore, considering the
356 significant contribution of autochthonous brGDGTs in Gahai lake, we also attempted to
357 reconstruct the Holocene paleotemperature record using previously published lake-specific
358 brGDGTs-temperature calibrations (e.g., Dang et al., 2018; Günther et al., 2014; Martínez-
359 Sosa et al., 2021; Russell et al., 2018; Sun et al., 2011; Wang et al., 2016). As illustrated in

设置了格式: 字体颜色: 蓝色

设置了格式: 字体颜色: 蓝色

360 Fig. S3, most of these calibrations showed qualitatively similar patterns of temperature
361 change when applied to the sediment core from Gahai lake. However, the magnitudes of
362 temperature fluctuations varied considerably and were found to be unsuitable for application
363 in Gahai lake due to several key reasons. Firstly, the fractional abundances of summed tetra-,
364 penta-, and hexamethylated brGDGTs in Gahai lake were inconsistent with those found in the
365 reference datasets (Fig. 4). Secondly, the analytical technique used for distinguishing 5- and
366 6-methyl isomers, which was a crucial aspect of some calibration studies (Günther et al.,
367 2014; Wang et al., 2016), was not employed in those studies, resulting in their exclusion from
368 our analysis. Thirdly, although the brGDGTs fractions in Gahai lake are resembled those of
369 East African lakes, the annual mean temperature reconstructed using this calibration

设置了格式: 字体颜色: 蓝色

设置了格式: 字体颜色: 蓝色

设置了格式: 字体颜色: 深红

设置了格式: 字体颜色: 蓝色

370 significantly differed from the temperature data recorded at the Langmu Temple station.
371 Moreover, even though the paleotemperature reconstruction for Gahai lake based on the
372 warm-season temperature calibration by Dang et al. (2018) showed similarity to the
373 calibration by Martínez-Sosa et al. (2021). However, it is worth noting that the calibration by
374 Dang et al. (2018) was established based on an investigation of 35 Chinese alkaline lakes,
375 which may not be directly applicable to the freshwater environment of Gahai lake. Similarly,
376 despite the salinity correction, the calibration reported by Wang et al. (2021) was not
377 considered suitable for our study.

设置了格式: 字体颜色: 蓝色

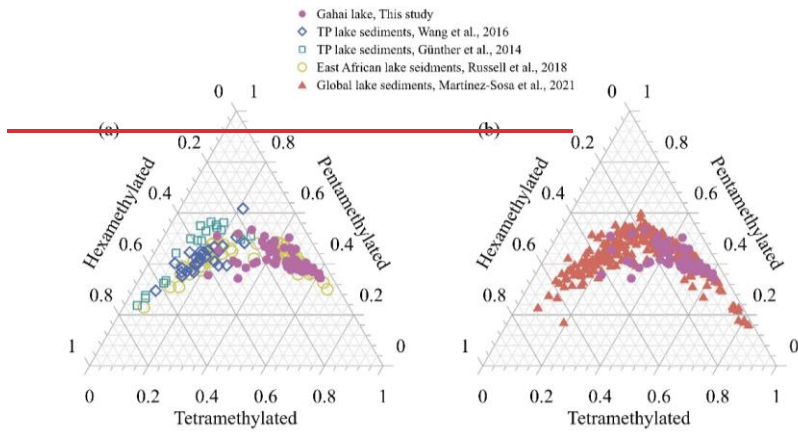
设置了格式: 字体颜色: 蓝色

设置了格式: 字体颜色: 蓝色

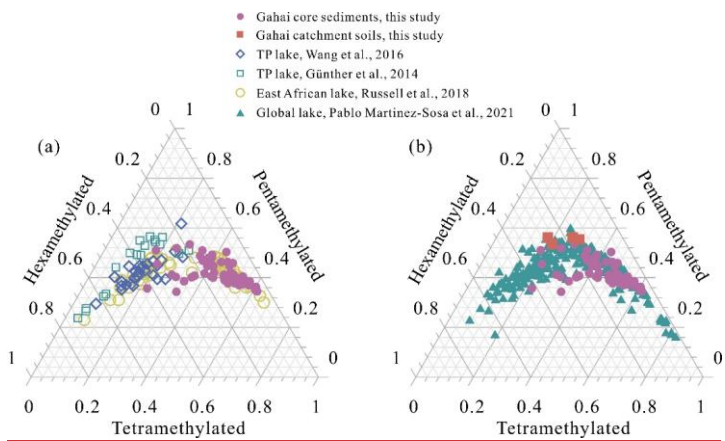
设置了格式: 字体颜色: 蓝色

378
379 ~~Given the substantial contribution of authigenic brGDGTs in the Gahai lake sediments, we~~
380 ~~reconstructed the Holocene paleotemperature record using previously published lake specific~~
381 ~~brGDGTs temperature calibrations (e.g., Sun et al., 2011; Günther et al., 2014; Wang et al.,~~
382 ~~2016; Dang et al., 2018; Russell et al., 2018; Martínez Sosa et al., 2021). As shown in Fig. S3,~~
383 ~~most calibrations produced qualitatively similar patterns of temperature change when applied~~
384 ~~to the sediment core from Gahai lake, but the amplitudes vary considerably. Among these~~
385 ~~calibrations, the reconstruction based on Martínez Sosa et al. (2021) was chosen to produce~~
386 ~~the final result, for several reasons. We compared the fractional abundances of summed tetra-,~~
387 ~~penta- and hexamethylated brGDGTs of Gahai lake with other datasets (Fig. 4), including~~
388 ~~lake sediments from the Tibetan Plateau (Günther et al., 2014; Wang et al., 2016), East Africa~~
389 ~~(Russell et al., 2018), and global lakes (Martínez Sosa et al., 2021). The fraction plot of the~~
390 ~~Gahai core sediments is clearly distinct from the other Tibetan Plateau lake sediments, even~~
391 ~~though they are all from the same region (Fig. 4), likely because the brGDGTs in Tibetan~~

392 lakes are mainly soil derived ((Wang et al., 2016). Moreover, the novel analytical technique
393 for separating 5 and 6 methyl isomers was not used in the studies of Wang et al. (2016) and
394 Günther et al. (2014), and thus these two calibrations were excluded. The fractional
395 distribution of brGDGTs in Gahai lake is spanned by that of global lakes, and based on
396 multiyear observed temperature records from the nearest meteorological station, the modern
397 mean temperature of the months with temperatures above freezing in Gahai lake (May to
398 September) was 8.8°C, which is like the brGDGT inferred temperature for the surficial
399 sediments (9.4°C), obtained using the calibration of Martínez Sosa et al. (2021). However,
400 the annual mean temperature reconstructed according to Russell et al. (2018) differs
401 significantly from that from Langmu Temple station, although the characteristics of the Gahai
402 brGDGTs fractions resemble those of East African lakes. The paleotemperature
403 reconstruction for Gahai lake based on the warm season temperature calibration proposed by
404 Dang et al. (2018) is similar to that of Martínez Sosa et al. (2021); however, this calibration
405 was established based on an investigation of 35 Chinese alkaline lakes, in contrast to
406 freshwater Gahai lake. Similarly, although the salinity effect was corrected, the calibration
407 reported by Wang et al. (2021b) is not considered here. Therefore, we used a new Bayesian
408 calibration for the mean temperature of the Months Above Freezing (Martínez Sosa et al.,
409 2021) to reconstruct a warm biased temperature for Gahai lake.



410



411

412 **Fig. 4** Comparison of the fractional abundances of tetramethylated, pentamethylated, and
 413 hexamethylated bGDGTs in sediment core samples from Gahai with lake surface
 414 sediments from the Tibetan Plateau (Günther et al., 2014; Wang et al., 2016), East Africa
 415 (Russell et al., 2018), and worldwide (Martínez-Sosa et al., 2021).

416 Given these limitations, we ultimately opted to use the new Bayesian calibration for the mean
 417 temperature of the Months Above Freezing, as proposed by Martínez-Sosa et al. (2021), to
 418 reconstruct a warm-biased temperature record for Gahai lake.

419

420 ~~Many studies have suggested that lacustrine brGDGTs derived temperatures are likely to~~
421 ~~have a warm season bias, especially in cold regions at middle to high latitudes (Shanahan et~~
422 ~~al., 2013; Peterse et al., 2014; Dang et al., 2018; Cao et al., 2020). However, for lakes in~~
423 ~~warmer regions, the reconstructed temperatures are much closer to the annual average~~
424 ~~temperature (Tierney et al., 2010; Loomis et al., 2012). Gahai is a shallow lake that is usually~~
425 ~~completely frozen during winter and spring, and the local meteorological data show that the~~
426 ~~average snowfall period is 269 days, and that the snowfall period lasts for ~50 days(Luqu~~
427 ~~County Local Chronicles Compilation Committee, 2006). Thus, the light transmittance and~~
428 ~~oxygen content during the lake water freezing season at Gahai are reduced, as well as the lake~~
429 ~~water nutrient contents, which seriously inhibit the growth of autotrophic microorganisms.~~
430 ~~Although the bacteria that produce brGDGTs are not well characterized, heterotrophic~~
431 ~~bacteria will be reduced by the decreased autotrophic biomass. (Sun et al., 2021; Zhang et al.,~~
432 ~~2022a)Therefore, we suggest that the brGDGTs based temperatures from Gahai are biased~~
433 ~~towards the growing season (summer and autumn).~~

434
435 The depth interval of 191–279 cm in the Gahai sediment core represents an interval of rapid
436 allocthonous sedimentation, or alternatively a slump, and therefore the results for the
437 corresponding time interval of 20–15 ka may be unreliable. Thus, our temperature record of
438 Months Above Freezing~~warm biased temperature record~~ from the eastern TP spans the past
439 15 ka, with the average temperature of 4°C, as shown in Fig. 5a. Within the range of age
440 uncertainties, weak warming occurred during 14.8–11.8 ka, likely to corresponding to the
441 Bølling–Allerød (B/A) interstadial. A minor cold reversal occurred during 11.8–10.5 ka,

设置了格式：字体颜色：深红

442 potentially corresponding to the Younger Dryas (YD) event. Notably, the samples collected
443 between 11.8 ka and 10.5 ka exhibited GDGT concentrations below the detection limit.
444 Therefore, we directly linked the temperature reconstructions at the two aforementioned time
445 points, ~11.8 ka and ~10.5 ka, resulting in the lowest temperature of this time period
446 appearing around 10.5 ka. This may cause a time lag with the occurrence of the YD event.
447 ~~Weak warming occurred during 14.8–11.8 ka which coincides with the Bølling–Allerød (B/A)~~
448 ~~interstadial, and a minor cold reversal occurred during 11.8–10.5 ka, which approximates the~~
449 ~~Younger Dryas (YD).~~ The temperature record indicates a colder period during 11.5–8.0 ka.
450 During 8.0–3.5 ka, Gahai experienced a stable warm period with the average temperature of
451 ~16.5°C, after which the temperature decreased gradually. Overall, the maximum temperature
452 difference since 15 ka was ~10°C. As for the absolute temperature changes since 15,000 yr,
453 although some influential studies indicate a warming of approximately 6.1–7°C from the
454 deglaciation onset to preindustrial times (Osman et al., 2021; Tierney et al., 2020). However,
455 these results are based on global mean sea surface temperatures. Our reconstructed
456 temperature range is about 10°C, considering the remarkable ‘elevation-dependent warming’
457 observed in high-altitude regions compared to low-altitude areas (Mountain Initiative EDW
458 Working Group, 2015). Thus, this range could be accurate. Nevertheless, we do not rule out
459 the possibility that our temperature reconstruction may exhibit an overestimation. This is a
460 known issue in temperature reconstruction using biomarkers. Aside from potential
461 uncertainties associated with the biomarkers themselves, calibrations may also considerably
462 influence the observed amplitude. We examined temperature variations reconstructed using
463 different calibrations (Fig. S3), with the smallest range being 6°C and the largest being 12°C.

设置了格式: 字体颜色: 深红

设置了格式: 字体颜色: 深红

设置了格式: 非突出显示

设置了格式: 非突出显示

域代码已更改

设置了格式: 非突出显示

设置了格式: 字体颜色: 深红

设置了格式: 字体颜色: 深红

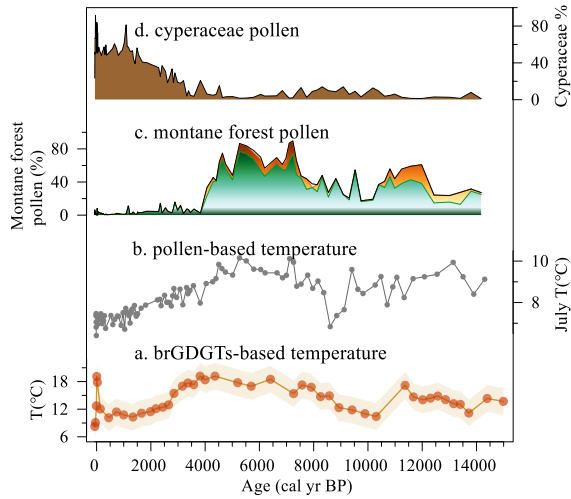
464 Undoubtedly, further efforts are needed to constrain the inherent uncertainties related to
465 biomarker-based temperature reconstructions. ~~The interval of 11.5–10.5 ka is represented by~~
466 ~~a relatively low number of samples because the concentration of brGDGTs was below the~~
467 ~~detection limit.~~

469 3.4 Holocene temperature changes on the eastern edge of TP and their origin

470 Despite the difference in amplitude, the temperature record of Months Above Freezing
471 ~~warm-biased temperature record~~ from Gahai resembles the pollen record and the pollen-
472 based temperature reconstruction from the same site (Fig. 5) (Wang et al., 2022). However,
473 the brGDGTs-based Holocene Thermal Maximum (HTM) lags the pollen-based
474 reconstruction (Fig. 5a, b). Wang et al. (2022) used a weighted-averaging partial least
475 regression approach to produce a temperature record for Gahai, based on a modern pollen
476 dataset (n=731) from the eastern TP. Assessment of the statistical significance of the pollen-
477 based climate variables for Gahai suggests that the mean July temperature is the most
478 important environmental factor influencing the fossil pollen assemblages. The brGDGTs in
479 Gahai are indicative of summer and autumn temperatures, and the mismatch between the
480 temperature records inferred from brGDGTs and the pollen record may be attributed to the
481 difference between the solar irradiance during June–October and that during July. A detailed
482 analysis of this topic will be undertaken in the subsequent section. ~~Additionally, significant~~
483 ~~vegetation changes occurred in the Gahai area during 4.0–3.5 ka, when the dominant high-~~
484 ~~elevation montane forest was rapidly replaced by alpine steppe. The poor vegetation coverage~~
485 ~~and lower soil moisture level during this period (Fig. 5c, d) (Wang et al., 2022) would have~~

设置了格式：字体颜色：深红

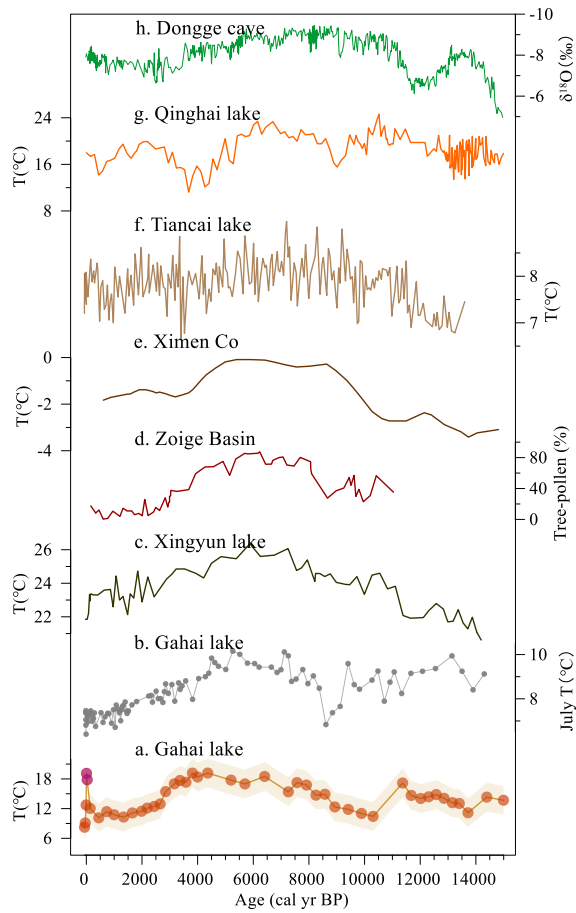
486 ~~resulted in more efficient heat absorption, causing surface warming (Lu et al., 2019).~~



487
488 **Fig. 5** Comparison of multiproxy records from Gahai lake. (a) brGDGTs-based warm-bias
489 temperature (this study). (b) Temperature of the warmest month (July) based on pollen
490 assemblages (Wang et al., 2022). (c, d) Pollen-reconstructed montane forest (*Pinus*,
491 *Picea*, *Abies*) and Cyperaceae pollen record (Wang et al., 2022).

492
493 ~~The brGDGTs-based temperature record from Gahai confirms the occurrence of a climate~~
494 ~~optimum in the mid-Holocene on the northeast Tibetan Plateau, which is consistent with~~
495 ~~several other pollen and pollen-reconstructed temperature records from the fringe areas of the~~
496 ~~Asian summer monsoon (Fig. 6), suggesting that it is a reliable representation of Holocene~~
497 ~~temperature changes in this region.~~The brGDGTs-based temperature record from Gahai is
498 also consistent with several other pollen and pollen-reconstructed temperature records from
499 the eastern TP (Fig. 6), suggesting that it is a reliable representation of Holocene temperature
500 changes in this region. For example, pollen-based temperature reconstructions from Xingyun

501 lake and Ximen Co on the eastern TP show a early to middle HTM (9–4 ka) and a cooling
502 trend thereafter (Fig. 6c, e) (Herzschuh et al., 2014; Wang et al., 2021a; Wu et al., 2018).
503 Additionally, lake water temperature reconstructions based on subfossil chironomids from
504 Tiancai lake (Fig. 6f) (Zhang et al., 2017; Zhang et al., 2019a) and alkenones from Qinghai
505 lake (Fig. 6g) (Hou et al., 2016) show the same trends during the past 15 ka, as also shown by
506 other pollen-based temperature records from the TP (Chen et al., 2020). Pollen, chironomids
507 and alkenones mainly respond to the growing season temperatures in middle and high
508 latitudes, and thus the reconstructed temperature records are consistent with the variations in
509 summer solar irradiance. Similar variations were documented in temperature reconstructions
510 at a global scale (Cartapanis et al., 2022; Marcott et al., 2013).

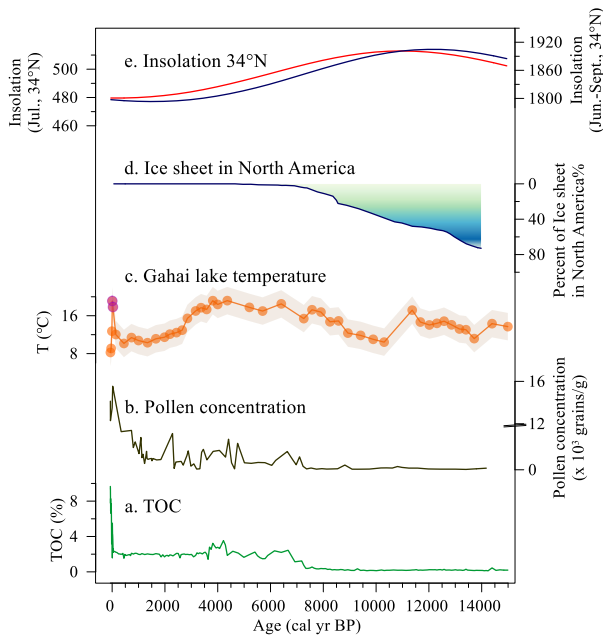


511

512 **Fig. 6** Comparison of temperature at Gahai and other records from the eastern edge of the
 513 Tibetan Plateau. (a) brGDGTs-based warm-bias temperature at Gahai, the purple dots
 514 may indicate unreliable temperature changes influenced by human activities (this study).
 515 (b) Temperature of the warmest month (July) based on pollen data from Gahai (Wang et
 516 al., 2022). (c) Pollen-based temperature at Xingyun lake (Wu et al., 2018). (d) Tree
 517 pollen percentages from the Hongyuan peatland in the southern Zoige Basin (Zhou et al.,
 518 2010). (e) Pollen-based temperature at Ximen Co (Herzschuh et al., 2014). (f)
 519 Chironomid-based temperature at Tiancai lake (Zhang et al., 2017, 2019a). (g)
 520 Alkenone-based temperature at Qinghai lake (Hou et al., 2016). (h) Stalagmite $\delta^{18}\text{O}$
 521 record of Dongge cave (Dykoski et al., 2005).

522

523 Nevertheless, the timing and amplitude of the Gahai temperature fluctuations differ from
524 those of other temperature records from this region (Fig. 6). These discrepancies may be the
525 result of the chronological uncertainties of these records, and to differences in the seasonal
526 and spatial responses to climate forcing and feedbacks. The temperature records shown in Fig.
527 6 mostly refer to summer temperatures, which are primarily influenced by summer insolation.



528

529 **Fig. 7** Temperature fluctuations and forcing factors during the Holocene. (a, b) TOC content
530 and pollen concentrations from Gahai (Wang et al., 2022). (c) brGDGTs-based warm-
531 bias temperature from Gahai, the purple dots may indicate unreliable temperature
532 changes influenced by human activities (this study). (d) Percentage of the remnant
533 Laurentide ice sheet in North America relative to the Last Glacial Maximum (Dyke,
534 2004). (e) Local insolation at 34 °N during ice-free months (Laskar et al., 2004).

535
536 The ~~warm-biased~~ temperature record in Gahai during the early Holocene fails to closely
537 track the Northern Hemisphere insolation trend, and there is also a time lag. The pollen-based
538 temperature record for Xingyun Lake in southwestern China also shows lower temperatures
539 in the early Holocene (Fig. 6c). The albedo effect caused by the increased cloud cover may be
540 the reason for the early Holocene decrease in summer temperatures (Wu et al., 2018).
541 However, the pollen record from Gahai indicates dry conditions during the early Holocene
542 (Wang et al., 2022), and cloud cover may not be the primary factor responsible for the low
543 temperatures at this time. The melting of Northern Hemisphere ice sheets during the early
544 Holocene weakened the Atlantic Meridional Overturning Circulation (AMOC) and
545 potentially also the global thermohaline circulation. This led to a reduction in the amount of
546 heat transport by the North Atlantic warm current to high-latitude regions, which resulted in
547 the low temperatures in middle to high latitudes of the Northern Hemisphere. The persistence
548 of the Laurentide ice sheet into the early Holocene maintained the regional albedo, as well as
549 discharging meltwater into the North Atlantic (Fig. 7d) (Dyke, 2004). ~~It is possible that these~~
550 ~~factors impacted the summer temperatures in the Indian Summer Monsoon (ISM) domain via~~
551 ~~ocean-atmosphere interactions.~~ In addition, a Holocene temperature simulation showed that
552 global warming was more pronounced when dust factors were excluded from the simulation
553 (Liu et al. (2018). The record of insoluble particles in the Greenland GISP2 ice core indicates
554 relatively high concentrations of atmospheric aerosols in the early Holocene (Zielinski and
555 Mershon, 1997), which would have weakened summer solar irradiation via radiative
556 feedback, leading to the cool temperatures during this period. These factors may together

557 have caused the early Holocene temperature decline at Gahai Lake, which slightly delayed
558 the onset of the Holocene Warm Period.

559

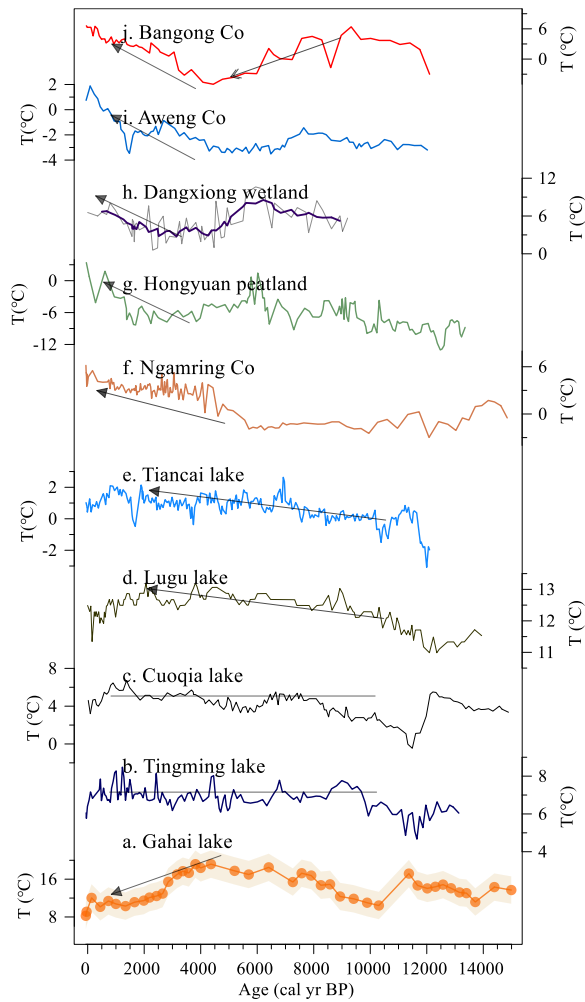
560 A ~~notable~~significant and rapid temperature increase is evident at Gahai in recent decades,
561 which differs ~~significantly~~ from the other records (Fig. 7c). Moreover, there are notable
562 increases in pollen concentration, TOC, and TN (Fig. 7a, b) in the Gahai sediment core,
563 indicating intensive local human activities like grazing and tourism, which may be the
564 primary cause of the environmental changes in this region (Wang et al., 2022). This intensive
565 human activity may have reduced the ability of the brGDGTs to record the natural
566 temperature background. ~~However, a series of environmental protection measures, including~~
567 ~~the government enforced exclusion of grazing, and a grassland restoration program, have~~
568 ~~been implemented to restore the natural ecological environment of this area. Consequently,~~
569 ~~the brGDGTs based temperature record decreased rapidly within the modern era, returning to~~
570 ~~normal levels, and it may provide a reliable regional record of the warm season temperature.~~
571 These observations emphasize the ~~significant~~important impact of human activities on climate
572 proxies and the need to carefully consider their effect on temperature reconstructions.

573

574 3.5 Spatiotemporal pattern of brGDGTs-based TP temperatures

575 In addition to comparing the Gahai temperature with the summer temperature records from
576 the eastern TP and its surrounding areas, we compiled and reviewed published Holocene
577 brGDGTs-based quantitative temperature records from across the TP. As shown in Fig. 8,
578 with the increasing number of these records for the TP, the differences between the results

579 have become more pronounced. The brGDGTs records from lakes in the central and western
580 parts of the plateau show higher temperatures in the early and late Holocene, and lower
581 temperatures in the middle Holocene (He et al., 2020; Li et al., 2017; Wang et al., 2021c),
582 while the brGDGTs records from lakes in the southern and south-eastern parts of the TP show
583 a warming trend throughout the Holocene (Feng et al., 2022; Sun et al., 2022). In addition,
584 brGDGTs in Cuoqia lake and Tingming lake, on the south-eastern TP, recorded the ice-free
585 season temperature, which was relatively stable during the Holocene (Sun et al., 2021; Zhang
586 et al., 2022a). However, our temperature record from Gahai is different from the above
587 records and resembles summer temperature changes during the Holocene (Chen et al., 2020).
588 This is because the brGDGTs record from Lake Gahai represents warm season temperatures,
589 which adds to its reliability.



590

591 **Fig. 8** Comparison of Holocene temperature based on brGDGTs at Gahai (a) and other
 592 records from around the TP. Reconstructed ice-free-season temperatures from (b)
 593 Tingming lake (Sun et al., 2021), (c) Cuoqia lake (Zhang et al., 2022a). Reconstructed
 594 annual temperature from (d) Lugu lake (Zhao et al., 2021b), (e) Tiancai lake (Feng et al.,
 595 2022), (f) Ngamring Co (Sun et al., 2022), (g) Hongyuan peatland (Yan et al., 2021). (h)
 596 Dangxiong wetland (Cheung et al., 2017), (i) Aweng Co (Li et al., 2017), (j) Bangong

597 Co (Wang et al., 2021c).

598

599 We suggest that the complexity of Holocene temperature patterns recorded by brGDGTs in
600 TP lakes is primarily due to the ambiguity of brGDGTs in these lakes, as well as to the spatial
601 heterogeneity of climate change across the TP. This ambiguity can be attributed to several
602 factors. First, the origin of brGDGTs in lakes remains an uncertain factor in temperature
603 reconstruction. An increasing number of studies indicate the occurrence of a significant
604 remarkable amount of autochthonous brGDGTs in lakes, but their abundance in soil can also
605 affect the distribution of brGDGTs in lakes due to their supply via soil erosion (e.g., Tierney
606 and Russell, 2009; Wang et al., 2023; Weber et al., 2015). In fact, even within the same lake
607 (e.g., Tengchongqinghai lake in southwestern China), two studies reached inconsistent
608 conclusions regarding the origin of brGDGTs (Tian et al., 2019; Zhao et al., 2021b), possibly
609 because the niches of certain brGDGTs may expand or contract compared to other locations
610 within a lake. Therefore, it is important to conduct detailed modern process studies to
611 accurately assess the sources of brGDGTs in lakes, especially with regard to evaluating the
612 proportion of autochthonous brGDGTs (Martin et al., 2020; Wang et al., 2023). Second,
613 brGDGTs may show a seasonal signal. Current brGDGTs–temperature calibrations for lakes
614 reflect the annual average temperature (De Jonge et al., 2014; Sun et al., 2011), as well as the
615 growing season temperature (Dang et al., 2018; Sun et al., 2011) and the ice-free season
616 temperature (Martínez-Sosa et al., 2021; Zhang et al., 2022a). Thus, there is no consensus
617 regarding whether the brGDGTs have a seasonal bias, and it is necessary to conduct
618 continuous, high-resolution seasonal investigations of lakes on the Tibetan Plateau to

619 comprehensively elucidate the seasonal characteristics of brGDGTs. This can enhance the
620 accuracy of regional temperature reconstruction and may help reconcile the complex
621 temperature patterns observed on the Tibetan Plateau. Third, the factors affecting the
622 distribution of brGDGTs in lakes are complex, including not only temperature, pH and
623 salinity but also oxygen content, water depth, and so on (Wang et al., 2021b; Wang et al.,
624 2016). The distribution of brGDGTs in lakes is significantly influenced by the hydrological
625 and physical properties of the lakes, and thus it is necessary to attain a more comprehensive
626 understanding of the characteristics of the lakes in the study area and their effects on
627 brGDGTs. Fourth, different brGDGTs–temperature calibrations may lead to
628 ~~markable~~ ~~significant~~ differences in both the amplitude and trend of temperature from the same
629 dataset (Feng et al., 2019; Wang et al., 2016). One reason for this is the deviation between in-
630 situ measured temperature and atmospheric temperature (Wang et al., 2020). Thus, selecting
631 an appropriate calibration and attempting to establish a brGDGTs-in situ temperature
632 calibration are effective means of enhancing the reliability of brGDGTs-based temperature
633 reconstructions.

634

635 **4 Conclusions**

636 We present a quantitative, brGDGTs-based seasonal paleotemperature record over the last 15
637 ka from the sediments of a shallow lake on the eastern Tibetan Plateau. Our reconstruction
638 resembles the summer temperature trend, with the Holocene Thermal Maximum occurring
639 during 8–3.5 ka. There is a lag between our brGDGTs-based reconstruction and pollen-based
640 July temperature recorded in the same sediment core, indicating a ~~significant~~ seasonal bias

641 between different proxies. Since 3.5 ka, the temperature decreased gradually, and the surficial
642 sediments reliably recorded the warm season temperature during the current period in the
643 Gahai Lake region. However, intensive local human activity during the last century has
644 affected the distribution of brGDGTs, resulting in temperature deviations recorded by
645 brGDGTs. However, the implementation of environmental protection policies have reduced
646 this anthropogenic signal. Our findings help better understand the seasonal signal of
647 brGDGTs in shallow lakes and provide important data for improving projections of terrestrial
648 climate change at high elevations.

649

650 We also investigated previously published brGDGTs-based Holocene temperature records on
651 the TP to determine the pattern of brGDGTs-based temperature changes and the possible
652 causes of the differences between reconstructions. We emphasize the need for the careful
653 examination of both the source and behavior of these compounds in lacustrine environments
654 and lake status, prior to the application of brGDGTs proxies in paleolimnological
655 reconstruction.

656

657 **Competing interests**

658 The contact author has declared that none of the authors has any competing interests.

659

660 **Acknowledgements**

661 This work was financially supported by the National Natural Science Foundation of China

662 ([42025103](#), 41877459) and the Second Tibetan Plateau Scientific Expedition and Research

663 (2019QZKK0601). We would like to thank Jan Bloemendal for the help with language

664 editing.

665

666 References

- 667
- 668 Bova, S., Rosenthal, Y., Liu, Z., Godad, S.P., Yan, M., 2021. Seasonal origin of the thermal
669 maxima at the Holocene and the last interglacial. *Nature* 589, 548-553.
- 670 Buckles, L.K., Weijers, J.W.H., Verschuren, D., Damste, J.S.S., 2014. Sources of core and
671 intact branched tetraether membrane lipids in the lacustrine environment: Anatomy of
672 Lake Challa and its catchment, equatorial East Africa. *Geochimica Et Cosmochimica*
673 *Acta* 140, 106-126.
- 674 Cao, J., Rao, Z., Shi, F., Jia, G., 2020. Ice formation on lake surfaces in winter causes warm-
675 season bias of lacustrine brGDGT temperature estimates. *Biogeosciences* 17, 2521-2536.
- 676 Cartapanis, O., Jonkers, L., Moffa-Sanchez, P., Jaccard, S.L., de Vernal, A., 2022. Complex
677 spatio-temporal structure of the Holocene Thermal Maximum. *Nat Commun* 13, 5662.
- 678 Chen, D., Xu, B., Yao, T., Guo, Z., Cui, P., Chen, F., Zhang, R., Zhang, X., Zhang, Y., Fan, J.,
679 Hou, Z., Zhang, T., 2015. Assessment of past, present and future environmental changes
680 on the Tibetan Plateau. *Chinese Science Bulletin* 60, 3025-3035.
- 681 Chen, F., Yu, Z., Yang, M., Ito, E., Wang, S., Madsen, D.B., Huang, X., Zhao, Y., Sato, T.,
682 Birks, H.J.B., Boomer, I., Chen, J., An, C., Wünnemann, B., 2008. Holocene moisture
683 evolution in arid central Asia and its out-of-phase relationship with Asian monsoon
684 history. *Quaternary Science Reviews* 27, 351-364.
- 685 Chen, F., Zhang, J., Liu, J., Cao, X., Hou, J., Zhu, L., Xu, X., Liu, X., Wang, M., Wu, D.,
686 Huang, L., Zeng, T., Zhang, S., Huang, W., Zhang, X., Yang, K., 2020. Climate change,
687 vegetation history, and landscape responses on the Tibetan Plateau during the Holocene:
688 A comprehensive review. *Quaternary Science Reviews* 243.
- 689 Chen, Y., Zheng, F., Yang, H., Yang, W., Wu, R., Liu, X., Liang, H., Chen, H., Pei, H., Zhang,
690 C., Pancost, R.D., Zeng, Z., 2022. The production of diverse brGDGTs by an
691 Acidobacterium providing a physiological basis for paleoclimate proxies. *Geochimica et*
692 *Cosmochimica Acta* 337, 155-165.
- 693 Cheung, M.-C., Zong, Y., Zheng, Z., Liu, Z., Aitchison, J.C., 2017. Holocene temperature and
694 precipitation variability on the central Tibetan Plateau revealed by multiple palaeo-
695 climatic proxy records from an alpine wetland sequence. *The Holocene* 27, 1669-1681.
- 696 Committee, L.C.L.C.C., 2006. Luqu County Chronicles. Gansu Cultural Publishing House,
697 Lanzhou.
- 698 Crampton-Flood, E.D., Tierney, J.E., Peterse, F., Kirkels, F.M.S.A., Damste, J.S.S., 2020.
699 BayMBT: A Bayesian calibration model for branched glycerol dialkyl glycerol
700 tetraethers in soils and peats. *Geochimica Et Cosmochimica Acta* 268, 142-159.
- 701 Dang, X., Ding, W., Yang, H., Pancost, R.D., Naafs, B.D.A., Xue, J., Lin, X., Lu, J., Xie, S.,
702 2018. Different temperature dependence of the bacterial brGDGT isomers in 35 Chinese
703 lake sediments compared to that in soils. *Organic Geochemistry* 119, 72-79.
- 704 De Jonge, C., Hopmans, E.C., Zell, C.I., Kim, J.-H., Schouten, S., Sinninghe Damsté, J.S.,
705 2014. Occurrence and abundance of 6-methyl branched glycerol dialkyl glycerol
706 tetraethers in soils: Implications for palaeoclimate reconstruction. *Geochimica et*
707 *Cosmochimica Acta* 141, 97-112.
- 708 Ding, S., Xu, Y., Wang, Y., He, Y., Hou, J., Chen, L., He, J.S., 2015. Distribution of branched
709 glycerol dialkyl glycerol tetraethers in surface soils of the Qinghai-Tibetan Plateau:

设置了格式: 字体: (默认) Times New Roman, 小四

带格式的: 缩进: 左侧: 0 厘米, 悬挂缩进: 2 字符,
首行缩进: -2 字符

710 implications of brGDGTs-based proxies in cold and dry regions. *Biogeosciences* 12,
711 3141-3151.

712 Dong, Y., Wu, N., Li, F., Zhang, D., Zhang, Y., Shen, C., Lu, H., 2022. The Holocene
713 temperature conundrum answered by mollusk records from East Asia. *Nat Commun* 13,
714 5153.

715 Dyke, A.S., 2004. An outline of North American deglaciation with emphasis on central and
716 northern Canada. *Quaternary Glaciations-Extent and Chronology, Pt 2: North America* 2,
717 373-424.

718 Dykoski, C.A., Edwards, R.L., Cheng, H., Yuan, D.X., Cai, Y.J., Zhang, M.L., Lin, Y.S., Qing,
719 J.M., An, Z.S., Revenaugh, J., 2005. A high-resolution, absolute-dated Holocene and
720 deglacial Asian monsoon record from Dongge Cave, China. *Earth and Planetary Science*
721 *Letters* 233, 71-86.

722 Feng, X., Zhao, C., D'Andrea, W.J., Liang, J., Zhou, A., Shen, J., 2019. Temperature
723 fluctuations during the Common Era in subtropical southwestern China inferred from
724 brGDGTs in a remote alpine lake. *Earth and Planetary Science Letters* 510, 26-36.

725 Feng, X., Zhao, C., D'Andrea, W.J., Hou, J., Yang, X., Xiao, X., Shen, J., Duan, Y., Chen, F.,
726 2022. Evidence for a Relatively Warm Mid - to Late Holocene on the Southeastern
727 Tibetan Plateau. *Geophysical Research Letters* 49.

728 Group, M.I.E.W., 2015. Elevation-dependent warming in mountain regions of the world.
729 *Nature Climate Change* 5, 424-430.

730 Günther, F., Thiele, A., Gleixner, G., Xu, B., Yao, T., Schouten, S., 2014. Distribution of
731 bacterial and archaeal ether lipids in soils and surface sediments of Tibetan lakes:
732 Implications for GDGT-based proxies in saline high mountain lakes. *Organic*
733 *Geochemistry* 67, 19-30.

734 Halamka, T.A., Raberg, J.H., McFarlin, J.M., Younkin, A.D., Mulligan, C., Liu, X.L., Kopf,
735 S.H., 2022. Production of diverse brGDGTs by *Acidobacterium Solibacter usitatus* in
736 response to temperature, pH, and O₂ provides a culturing perspective on brGDGT
737 proxies and biosynthesis. *Geobiology*.

738 He, Y., Hou, J., Wang, M., Li, X., Liang, J., Xie, S., Jin, Y., 2020. Temperature Variation on
739 the Central Tibetan Plateau Revealed by Glycerol Dialkyl Glycerol Tetraethers From the
740 Sediment Record of Lake Linggo Co Since the Last Deglaciation. *Frontiers in Earth*
741 *Science* 8.

742 Herzschuh, U., Borkowski, J., Schewe, J., Mischke, S., Tian, F., 2014. Moisture-advection
743 feedback supports strong early-to-mid Holocene monsoon climate on the eastern Tibetan
744 Plateau as inferred from a pollen-based reconstruction. *Palaeogeography,*
745 *Palaeoclimatology, Palaeoecology* 402, 44-54.

746 Hou, J., Huang, Y., Zhao, J., Liu, Z., Colman, S., An, Z., 2016. Large Holocene summer
747 temperature oscillations and impact on the peopling of the northeastern Tibetan Plateau.
748 *Geophysical Research Letters* 43, 1323-1330.

749 Hou, J., Li, C., Lee, S., 2019. The temperature record of the Holocene: progress and
750 controversies. *Science Bulletin*.

751 Hugué, C., Hopmans, E.C., Febo-Ayala, W., Thompson, D.H., Sinninghe Damsté, J.S.,
752 Schouten, S., 2006. An improved method to determine the absolute abundance of
753 glycerol dibiphytanyl glycerol tetraether lipids. *Organic Geochemistry* 37, 1036-1041.

- 754 Kuang, X., Jiao, J.J., 2016. Review on climate change on the Tibetan Plateau during the last
755 half century. *Journal of Geophysical Research: Atmospheres* 121, 3979-4007.
- 756 Laskar, J., Robutel, P., Joutel, F., Gastineau, M., Correia, A.C.M., Levrard, B., 2004. A long-
757 term numerical solution for the insolation quantities of the Earth. *Astronomy &*
758 *Astrophysics* 428, 261-285.
- 759 Li, X., Wang, M., Zhang, Y., Lei, L., Hou, J., 2017. Holocene climatic and environmental
760 change on the western Tibetan Plateau revealed by glycerol dialkyl glycerol tetraethers
761 and leaf wax deuterium-to-hydrogen ratios at Aweng Co. *Quaternary Research* 87, 455-
762 467.
- 763 Liu, Y., Zhang, M., Liu, Z., Xia, Y., Huang, Y., Peng, Y., Zhu, J., 2018. A Possible Role of
764 Dust in Resolving the Holocene Temperature Conundrum. *Scientific Reports* 8.
- 765 Liu, Z.Y., Zhu, J., Rosenthal, Y., Zhang, X., Otto-Bliesner, B.L., Timmermann, A., Smith,
766 R.S., Lohmann, G., Zheng, W.P., Timm, O.E., 2014. The Holocene temperature
767 conundrum. *Proc. Natl. Acad. Sci. U. S. A.* 111, E3501-E3505.
- 768 Loomis, S.E., Russell, J.M., Heuroux, A.M., D'Andrea, W.J., Sinninghe Damsté, J.S., 2014.
769 Seasonal variability of branched glycerol dialkyl glycerol tetraethers (brGDGTs) in a
770 temperate lake system. *Geochimica et Cosmochimica Acta* 144, 173-187.
- 771 Lu, H., Wu, N., Liu, K.-b., Zhu, L., Yang, X., Yao, T., Wang, L., Li, Q., Liu, X., Shen, C., Li,
772 X., Tong, G., Jiang, H., 2011. Modern pollen distributions in Qinghai-Tibetan Plateau
773 and the development of transfer functions for reconstructing Holocene environmental
774 changes. *Quaternary Science Reviews* 30, 947-966.
- 775 Ma, W., Li, G., Song, J., Yan, L., Wu, L., 2019. Effect of Vegetation Degradation on Soil
776 Organic Carbon Pool and Carbon Pool Management Index in the Gahai Wetland, China.
777 *Acta Agrestia Sinica* 27, 687-694.
- 778 Marcott, S.A., Shakun, J.D., Clark, P.U., Mix, A.C., 2013. A Reconstruction of Regional and
779 Global Temperature for the Past 11,300 Years. *Science* 339, 1198-1201.
- 780 Marsicek, J., Shuman, B.N., Bartlein, P.J., Shafer, S.L., Brewer, S., 2018. Reconciling
781 divergent trends and millennial variations in Holocene temperatures. *Nature* 554, 92-+.
- 782 Martin, C., Ménot, G., Thouveny, N., Peyron, O., Andrieu-Ponel, V., Montade, V., Davtian,
783 N., Reille, M., Bard, E., 2020. Early Holocene Thermal Maximum recorded by branched
784 tetraethers and pollen in Western Europe (Massif Central, France). *Quaternary Science*
785 *Reviews* 228, 106109.
- 786 Martínez-Sosa, P., Tierney, J.E., Stefanescu, I.C., Dearing Crampton-Flood, E., Shuman, B.N.,
787 Routson, C., 2021. A global Bayesian temperature calibration for lacustrine brGDGTs.
788 *Geochimica et Cosmochimica Acta* 305, 87-105.
- 789 Moser, K.A., Baron, J.S., Brahney, J., Oleksy, I.A., Saros, J.E., Hundey, E.J., Sadro, S.,
790 Kopáček, J., Sommaruga, R., Kainz, M.J., Strecker, A.L., Chandra, S., Walters, D.M.,
791 Preston, D.L., Michelutti, N., Lepori, F., Spaulding, S.A., Christianson, K.R., Melack,
792 J.M., Smol, J.P., 2019. Mountain lakes: Eyes on global environmental change. *Global*
793 *and Planetary Change* 178, 77-95.
- 794 Opitz, S., Zhang, C., Herzschuh, U., Mischke, S., 2015. Climate variability on the south-
795 eastern Tibetan Plateau since the Lateglacial based on a multiproxy approach from Lake
796 Naleng – comparing pollen and non-pollen signals. *Quaternary Science Reviews* 115,
797 112-122.

798 Osman, M.B., Tierney, J.E., Zhu, J., Tardif, R., Hakim, G.J., King, J., Poulsen, C.J., 2021.
799 Globally resolved surface temperatures since the Last Glacial Maximum. *Nature* 599,
800 239-244.

801 Pang, H., Hou, S., Zhang, W., Wu, S., Jenk, T.M., Schwikowski, M., Jouzel, J., 2020.
802 Temperature Trends in the Northwestern Tibetan Plateau Constrained by Ice Core Water
803 Isotopes Over the Past 7,000 Years. *Journal of Geophysical Research-Atmospheres* 125.

804 Qiu, J., 2008. The third pole. *Nature* 454, 393-396.

805 Russell, J.M., Hopmans, E.C., Loomis, S.E., Liang, J., Sinninghe Damsté, J.S., 2018.
806 Distributions of 5- and 6-methyl branched glycerol dialkyl glycerol tetraethers
807 (brGDGTs) in East African lake sediment: Effects of temperature, pH, and new
808 lacustrine paleotemperature calibrations. *Organic Geochemistry* 117, 56-69.

809 Sinninghe Damsté, J.S., Hopmans, E.C., Pancost, R.D., Schouten, S., Geenevasen, J.A.J.,
810 2000. Newly discovered non-isoprenoid glycerol dialkyl glycerol tetraether lipids in
811 sediments. *Chemical Communications*, 1683-1684.

812 Sinninghe Damsté, J.S., Ossebaar, J., Abbas, B., Schouten, S., Verschuren, D., 2009. Fluxes
813 and distribution of tetraether lipids in an equatorial African lake: Constraints on the
814 application of the TEX86 palaeothermometer and BIT index in lacustrine settings.
815 *Geochimica et Cosmochimica Acta* 73, 4232-4249.

816 Sun, Q., Chu, G., Liu, M., Xie, M., Li, S., Ling, Y., Wang, X., Shi, L., Jia, G., Lü, H., 2011.
817 Distributions and temperature dependence of branched glycerol dialkyl glycerol
818 tetraethers in recent lacustrine sediments from China and Nepal. *Journal of Geophysical
819 Research* 116.

820 Sun, X., Zhao, C., Zhang, C., Feng, X., Yan, T., Yang, X., Shen, J., 2021. Seasonality in
821 Holocene Temperature Reconstructions in Southwestern China. *Paleoceanography and
822 Paleoclimatology* 36.

823 Sun, Z., Hou, X., Ji, K., Yuan, K., Li, C., Wang, M., Hou, J., 2022. Potential winter-season
824 bias of annual temperature variations in monsoonal Tibetan Plateau since the last
825 deglaciation. *Quaternary Science Reviews* 292.

826 Thompson, L.G., Yao, T., Davis, M.E., Henderson, K.A., MosleyThompson, E., Lin, P.N.,
827 Beer, J., Synal, H.A., ColeDai, J., Bolzan, J.F., 1997. Tropical climate instability: The
828 last glacial cycle from a Qinghai-Tibetan ice core. *Science* 276, 1821-1825.

829 Tian, L., Wang, M., Zhang, X., Yang, X., Zong, Y., Jia, G., Zheng, Z., Man, M., 2019.
830 Synchronous change of temperature and moisture over the past 50 ka in subtropical
831 southwest China as indicated by biomarker records in a crater lake. *Quaternary Science
832 Reviews* 212, 121-134.

833 Tierney, J.E., Russell, J.M., 2009. Distributions of branched GDGTs in a tropical lake system:
834 Implications for lacustrine application of the MBT/CBT paleoproxy. *Organic
835 Geochemistry* 40, 1032-1036.

836 Tierney, J.E., Russell, J.M., Eggermont, H., Hopmans, E.C., Verschuren, D., Sinninghe
837 Damsté, J.S., 2010. Environmental controls on branched tetraether lipid distributions in
838 tropical East African lake sediments. *Geochimica et Cosmochimica Acta* 74, 4902-4918.

839 Tierney, J.E., Zhu, J., King, J., Malevich, S.B., Hakim, G.J., Poulsen, C.J., 2020. Glacial
840 cooling and climate sensitivity revisited. *Nature* 584, 569-+.

841 van Bree, L.G.J., Peterse, F., Baxter, A.J., De Crop, W., van Grinsven, S., Villanueva, L.,

842 Verschuren, D., Sinninghe Damsté, J.S., 2020. Seasonal variability and sources of in situ
843 brGDGT production in a permanently stratified African crater lake. *Biogeosciences* 17,
844 5443-5463.

845 Wang, G., Wang, Y., Wei, Z., He, W., Ma, X., Zhang, T., 2021a. Reconstruction of
846 temperature and precipitation spanning the past 28 kyr based on branched tetraether
847 lipids from Qionghai Lake, southwestern China. *Palaeogeography Palaeoclimatology*
848 *Palaeoecology* 562.

849 Wang, H., An, Z., Lu, H., Zhao, Z., Liu, W., 2020. Calibrating bacterial tetraether
850 distributions towards in situ soil temperature and application to a loess-paleosol
851 sequence. *Quaternary Science Reviews* 231.

852 Wang, H., Liu, W., He, Y., Zhou, A., Zhao, H., Liu, H., Cao, Y., Hu, J., Meng, B., Jiang, J.,
853 Kolpakova, M., Krivonogov, S., Liu, Z., 2021b. Salinity-controlled isomerization of
854 lacustrine brGDGTs impacts the associated MBT5ME' terrestrial temperature index.
855 *Geochimica et Cosmochimica Acta* 305, 33-48.

856 Wang, H., Chen, W., Zhao, H., Cao, Y., Hu, J., Zhao, Z., Cai, Z., Wu, S., Liu, Z., Liu, W.,
857 2023. Biomarker-based quantitative constraints on maximal soil-derived brGDGTs in
858 modern lake sediments. *Earth and Planetary Science Letters* 602.

859 Wang, M., Liang, J., Hou, J., Hu, L., 2016. Distribution of GDGTs in lake surface sediments
860 on the Tibetan Plateau and its influencing factors. *Science China Earth Sciences* 59, 961-
861 974.

862 Wang, M.D., Hou, J.Z., Duan, Y.W., Chen, J.H., Li, X.M., He, Y., Lee, S.Y., Chen, F.H.,
863 2021c. Internal feedbacks forced Middle Holocene cooling on the Qinghai-Tibetan
864 Plateau. *Boreas*.

865 Wang, N., Liu, L., Hou, X., Zhang, Y., Wei, H., Cao, X., 2022. Palynological evidence reveals
866 an arid early Holocene for the northeast Tibetan Plateau. *Climate of the Past* 18, 2381-
867 2399.

868 Weber, Y., De Jonge, C., Rijpstra, W.I.C., Hopmans, E.C., Stadnitskaia, A., Schubert, C.J.,
869 Lehmann, M.F., Sinninghe Damsté, J.S., Niemann, H., 2015. Identification and carbon
870 isotope composition of a novel branched GDGT isomer in lake sediments: Evidence for
871 lacustrine branched GDGT production. *Geochimica et Cosmochimica Acta* 154, 118-129.

872 Weber, Y., Sinninghe Damsté, J.S., Zopfi, J., De Jonge, C., Gilli, A., Schubert, C.J., Lepori, F.,
873 Lehmann, M.F., Niemann, H., 2018. Redox-dependent niche differentiation provides
874 evidence for multiple bacterial sources of glycerol tetraether lipids in lakes. *Proc Natl*
875 *Acad Sci U S A* 115, 10926-10931.

876 Weijers, J.W.H., Schouten, S., van den Donker, J.C., Hopmans, E.C., Sinninghe Damsté, J.S.,
877 2007. Environmental controls on bacterial tetraether membrane lipid distribution in soils.
878 *Geochimica et Cosmochimica Acta* 71, 703-713.

879 Woltering, M., Werne, J.P., Kish, J.L., Hicks, R., Sinninghe Damsté, J.S., Schouten, S., 2012.
880 Vertical and temporal variability in concentration and distribution of thaumarchaeotal
881 tetraether lipids in Lake Superior and the implications for the application of the TEX86
882 temperature proxy. *Geochimica et Cosmochimica Acta* 87, 136-153.

883 Wu, D., Chen, X., Lv, F., Brenner, M., Curtis, J., Zhou, A., Chen, J., Abbott, M., Yu, J., Chen,
884 F., 2018. Decoupled early Holocene summer temperature and monsoon precipitation in
885 southwest China. *Quaternary Science Reviews* 193, 54-67.

886 Wu, J., Yang, H., Pancost, R.D., Naafs, B.D.A., Qian, S., Dang, X., Sun, H., Pei, H., Wang,
887 R., Zhao, S., Xie, S., 2021. Variations in dissolved O₂ in a Chinese lake drive changes in
888 microbial communities and impact sedimentary GDGT distributions. *Chemical Geology*
889 579.

890 Yan, T., Zhao, C., Yan, H., Shi, G., Sun, X., Zhang, C., Feng, X., Leng, C., 2021. Elevational
891 differences in Holocene thermal maximum revealed by quantitative temperature
892 reconstructions at ~30° N on eastern Tibetan Plateau. *Palaeogeography,
893 Palaeoclimatology, Palaeoecology* 570, 110364.

894 Yao, T., Bolch, T., Chen, D., Gao, J., Immerzeel, W., Piao, S., Su, F., Thompson, L., Wada, Y.,
895 Wang, L., Wang, T., Wu, G., Xu, B., Yang, W., Zhang, G., Zhao, P., 2022. The imbalance
896 of the Asian water tower. *Nature Reviews Earth & Environment* 3, 618-632.

897 Zhang, C., Zhao, C., Yu, S.-Y., Yang, X., Cheng, J., Zhang, X., Xue, B., Shen, J., Chen, F.,
898 2022a. Seasonal imprint of Holocene temperature reconstruction on the Tibetan Plateau.
899 *Earth-Science Reviews* 226, 103927.

900 Zhang, E., Chang, J., Cao, Y., Sun, W., Shulmeister, J., Tang, H., Langdon, P.G., Yang, X.,
901 Shen, J., 2017. Holocene high-resolution quantitative summer temperature
902 reconstruction based on subfossil chironomids from the southeast margin of the
903 Qinghai-Tibetan Plateau. *Quaternary Science Reviews* 165, 1-12.

904 Zhang, E., Chang, J., Shulmeister, J., Langdon, P., Sun, W., Cao, Y., Yang, X., Shen, J., 2019a.
905 Summer temperature fluctuations in Southwestern China during the end of the LGM and
906 the last deglaciation. *Earth and Planetary Science Letters* 509, 78-87.

907 Zhang, G., Luo, W., Chen, W., Zheng, G., 2019b. A robust but variable lake expansion on the
908 Tibetan Plateau. *Science Bulletin* 64, 1306-1309.

909 Zhang, W., Wu, H., Cheng, J., Geng, J., Li, Q., Sun, Y., Yu, Y., Lu, H., Guo, Z., 2022b.
910 Holocene seasonal temperature evolution and spatial variability over the Northern
911 Hemisphere landmass. *Nat Commun* 13, 5334.

912 Zhao, B., Castaneda, I.S., Bradley, R.S., Salacup, J.M., de Wet, G.A., Daniels, W.C.,
913 Schneider, T., 2021a. Development of an in situ branched GDGT calibration in Lake 578,
914 southern Greenland. *Organic Geochemistry* 152.

915 Zhao, C., Liu, Z.H., Rohling, E.J., Yu, Z.C., Liu, W.G., He, Y.X., Zhao, Y., Chen, F.H., 2013.
916 Holocene temperature fluctuations in the northern Tibetan Plateau. *Quaternary Research*
917 80, 55-65.

918 Zhao, C., Rohling, E.J., Liu, Z., Yang, X., Zhang, E., Cheng, J., Liu, Z., An, Z., Yang, X.,
919 Feng, X., Sun, X., Zhang, C., Yan, T., Long, H., Yan, H., Yu, Z., Liu, W., Yu, S.-Y., Shen,
920 J., 2021b. Possible obliquity-forced warmth in southern Asia during the last glacial stage.
921 *Science Bulletin* 66, 1136-1145.

922 Zheng, Y., Li, Q., Wang, Z., Naafs, B.D.A., Yu, X., Pancost, R.D., 2015. Peatland GDGT
923 records of Holocene climatic and biogeochemical responses to the Asian Monsoon.
924 *Organic Geochemistry* 87, 86-95.

925 Zhou, W., Yu, S.-Y., Burr, G.S., Kukla, G.J., Jull, A.J.T., Xian, F., Xiao, J., Colman, S.M., Yu,
926 H., Liu, Z., Kong, X., 2010. Postglacial changes in the Asian summer monsoon system:
927 a pollen record from the eastern margin of the Tibetan Plateau. *Boreas* 39, 528-539.

928 Zielinski, G.A., Mershon, G.R., 1997. Paleoenvironmental implications of the insoluble
929 microparticle record in the GISP2 (Greenland) ice core during the rapidly changing

930 climate of the Pleistocene-Holocene transition. Geological Society of America Bulletin
931 109, 547-559.

932

933